Journal of The Electrochemical Society, **157** (10) B1391-B1396 (2010)
0013-4651/2010/157(10)/B1391/6/$28.00 © The Electrochemical Society

Study of Alkaline Electrodes for Hybrid Polymer Electrolyte Fuel Cells

Murat Ünlü,[*] Junfeng Zhou,[**] and Paul A. Kohl[*,z]**

School of Chemical and Biomolecular Engineering, Georgia Institute of Technology, Atlanta, Georgia 30332-0100, USA

Hybrid polymer electrolyte fuel cells combine a proton exchange membrane (PEM) and anion exchange membrane (AEM) and exhibit unique advantages. The electrochemical performance and current limitations of a hybrid cell with an alkaline electrode fabricated on a Nafion membrane was characterized at 70°C as a function of relative humidity. To separate the individual characteristics of the AEM anode and cathode electrodes, two semihybrid cell configurations, each with an AEM and PEM electrode, were constructed and compared to a conventional PEM fuel cell. Electrochemical impedance spectroscopy was used to diagnose the cell component characteristics. In particular, low catalyst utilization in the AEM electrode was a primary factor in the performance losses in the hybrid cells.
 [DOI: 10.1149/1.3468700]

Manuscript submitted March 9, 2010; revised manuscript received June 29, 2010. Published August 9, 2010.

Anion exchange membrane (AEM) fuel cells have recently received attention due to their advantages over traditional proton exchange membrane (PEM) fuel cells.[1] High pH in the AEM fuel cell enables the use of nonplatinum metals as catalysts and provides enhanced resistance to CO poisoning.[2,3] Although AEM-based fuel cells offer several advantages compared to PEM cells, the lower ionic conductivity of an AEM compared to commercially available PEMs (e.g., Nafion) and the dependence on relative humidity (RH) of the reactants remain a barrier to achieving high performance in current AEM fuel cells.[4]

To address the current challenges of PEM and AEM fuel cells, we recently developed a hybrid polymer electrolyte fuel cell that includes both AEM and PEM materials in a single cell design.[5,6] The configuration of the hybrid polymer electrolyte fuel cell with alkaline electrodes and acidic membrane is shown in Fig. 1. This hybrid design utilizes a high conductivity PEM as a core and exploits the advantages of high pH AEM electrodes. A critical aspect of the hybrid cell is the creation of a junction at the interface between the AEM and PEM regions of the cell. The junction potentials formed at the PEM/AEM interface constitute a perturbation to the Nernst potential.[7] Because these two junctions are in the opposite direction, the junction potentials of each cancel and result in a thermodynamic cell voltage of 1.23 V for hydrogen and oxygen at standard temperature and pressure. When only one AEM/PEM junction exists, its potential is exactly offset by the pH change in the Nernst equation at the two electrodes again producing a thermodynamic voltage of 1.23 V, as discussed in Ref. 7.

The mobile ions migrate in the opposite direction in the AEM and PEM regions of the cell to maintain charge neutrality in the electrodes. Cations migrate to the right in the PEM while anions migrate to the left in the AEM. This causes water to dissociate at the AEM anode/PEM interface (left side of the cell in Fig. 1) and water to be formed at the PEM/AEM cathode interface (right side of the cell in Fig. 1).[7] This unusual behavior at the AEM/PEM interfaces significantly changes the operating dynamics of the fuel cell. In the working cell, water is generated in two regimes within the membrane electrode assembly (MEA): (*i*) within the anode layer where hydrogen is oxidized and the protons combine with the mobile hydroxide and (*ii*) at the PEM/cathode junction, where hydroxide in the AEM combine with protons in the PEM. In addition, water is consumed in two regions: (*i*) within the cathode layer where oxygen is reduced in the presence of water to form hydroxide and (*ii*) at the PEM/anode junction where water dissociates. This is significantly different than a traditional PEM fuel cell, where water is generated at the cathode (product of oxygen reduction). It is also different from an AEM fuel cell, where water is formed within the anode layer and consumed at the cathode. The dynamics in the hybrid cell offer an opportunity to better control or possibly simplify water management compared to a single-material cell.

Although the prospects of hybrid cells are significant, the preliminary cell performance (78.3 mW/cm^2 for H_2/O_2 at 60°C) was moderate compared to PEM fuel cells.[6] It is essential to understand the origin of performance losses so as to improve the performance of hybrid cells. In this study, the electrochemical performance of a hybrid cell with alkaline electrodes was characterized at 70°C as a function of RH. Two semihybrid cell configurations with AEM and PEM electrodes were constructed and compared to a conventional PEM fuel cell to identify the individual characteristics of the AEM electrodes at the anode and cathode. The semihybrid configuration has only one AEM electrode, as compared to the full-hybrid case shown in Fig. 1. Electrochemical impedance spectroscopy (EIS) was used to diagnose the impedance of cell components in the semihybrid configuration. The effect of catalyst utilization was investigated in the EIS studies.

Experimental

High pH electrode (AEM electrode) was made using an anion exchange ionomer (AEI), poly(arylene ether sulfone) functionalized with quaternary ammonium groups synthesized for this study, as described previously.[8] The physical properties of the AEM are summarized in Table I. The AEI was stored as a 5 wt % solution in dimethylformamide (DMF). The Nafion membranes were pretreated with 3% H_2O_2 and 1 M H_2SO_4 before use.

The catalyst ink for the PEM electrode was prepared by mixing Nafion solution (5% dispersion), Pt/C catalyst (20% Pt on carbon, E-TEK), isopropyl alcohol (IPA), and water. The catalyst ink for the anionic, high pH AEM electrode was prepared by mixing the Pt/C catalyst and the AEI with a mixture of water and DMF (2:3 weight ratio). The catalyst inks were sonicated for 15 min and then cast onto hydrophobic Toray carbon paper (TGPH-090). The resulting electrodes had a surface area of 2 cm^2 and catalyst loading of 0.5 mg/cm^2.

Once the electrodes were dry, 50 μL of AEI in DMF (1 wt %) was sprayed directly onto the surface of the AEM electrode. The purpose of this additional AEI layer was to prevent contact between the catalyst in the AEM electrode and the PEM membrane. Thus, a high pH environment in the electrode reaction domain was ensured. After drying at room temperature, the AEM electrodes were immersed in aqueous 0.1 M KOH to exchange OH^- for Cl^-. 100 μL of the Nafion (5% suspension):IPA mixture (1:2 by volume) was sprayed onto the AEM electrodes before assembling the electrodes onto the membrane. The AEM electrodes were pressed onto Nafion 212 at 2 MPa gauge pressure and ambient temperature for 3 min.

* Electrochemical Society Student Member.
** Electrochemical Society Active Member.
*** Electrochemical Society Fellow.
z E-mail: kohl@gatech.edu

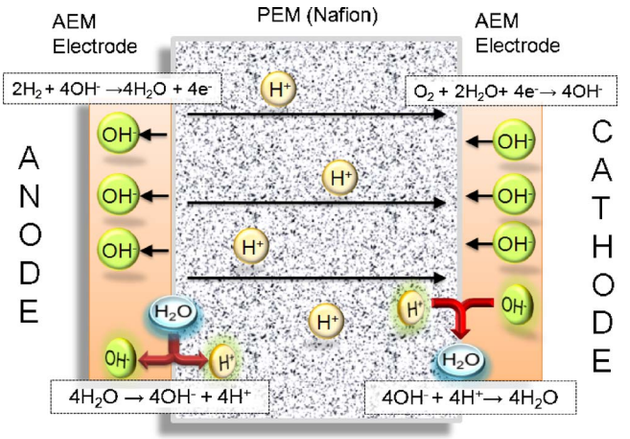

Figure 1. (Color online) Configuration of a hybrid fuel cell comprised of two high pH AEM electrodes on a low pH proton-conducting membrane.

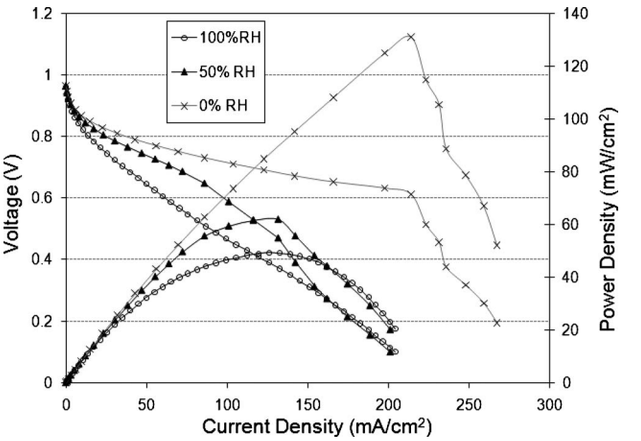

Figure 2. Current density vs cell voltage and power density of the hybrid fuel cell at 70°C and 0, 50, and 100% RH values. The anode and cathode flow rates were 6 sccm H_2 and 8 sscm O_2.

For the semihybrid cells with one PEM electrode and one AEM electrode, the MEA was assembled in two steps. In the first step, the PEM electrode was pressed onto Nafion 212 at 2 MPa gauge pressure and 135°C temperature for 3 min. In the second step, the AEM electrode was pressed onto the PEM half-cell assembly at 2 MPa and ambient temperature for 3 min. Conventional PEM-based MEAs were prepared by the following protocol: 100 μL of the Nafion (5% suspension):IPA mixture (1:2 by volume) was first sprayed onto the PEM electrode. The PEM electrodes were then pressed onto Nafion 212 at 2 MPa gauge pressure and 135°C temperature for 3 min.

The fuel cell hardware assembly (Fuel Cell Technologies) consisted of a pair of Poco graphite blocks with a single-serpentine flow pattern. All MEAs were preconditioned by operating at steady state at 600 mV discharge voltage for 24 h before performing current–voltage (*I-V*) polarization experiments. Electrochemical measurements were performed using a PAR 2273 potentiostat/galvanostat. All fuel cell tests were conducted at ambient pressure. EIS was used to follow the cell performance along with polarization curves in the potentiostatic mode. The EIS experiments used frequencies from 10 mHz–10 kHz. The amplitude of the ac voltage was 10 mV.

Results and Discussion

The performance of the hybrid MEA was evaluated using H_2 fuel at the anode and O_2 at the cathode at 70°C. The *I-V* curves are shown in Fig. 2 as a function of RH. The *I-V* curves were subject to normal variation in reproducibility in fuel cell electrode construction and performance. The data was collected after 24 h of steady-state operation. The RH was changed symmetrically for both the anode and cathode inlet gases. The performance increased as the RH decreased. The maximum power densities were 49, 62, and 131 mW/cm^2 for the RH values of 100, 50, and 0%, respectively. This behavior is contrary to that of a conventional AEM or PEM fuel cell. Typically, the performance of a conventional fuel cell increases with RH because ionic conductivity of the polymer electrolyte improves with RH. The highest current and power were observed at 0% RH; however, a critical current was reached at ca. 220 mA/cm^2 where the current deviated sharply from the expected *I-V* behavior and the power dropped, Fig. 2. This behavior is shown to be tied to water management within the membrane.

EIS was used to analyze the performance of the cells. The impedance spectra were measured at 600 mV for the 0, 50, and 100% RH experiments at 70°C. The Nyquist plots (imaginary component of the impedance vs the real component of the impedance) are shown in Fig. 3. The high frequency end of the plot occurs at low values of the real impedance and the low frequency end is at the right side of the plot in Fig. 3. The spectra are single loops for each RH with a distortion in shape. At high frequencies, the plot deviates from semicircular with a linear end as the data approaches the *x*-intercept (left side of the spectrum). The single loop, commonly defined as medium-*f* feature, represents the charge-transfer resistance (R_{CT}) in parallel with the double layer capacitance.[9-11] The linear branch at high frequency at the left side of the plot (ca. 45° angle to the *x*-axis) is attributed to a distributed ohmic resistance and capacitive behavior in the porous catalyst layer. The resistive component of this distributed resistance–capacitance (RC) network within the electrode structure can be captured by a single value in Fig. 3, $R_{D\Omega}$.[9] The electrode is not a planar electrode represented by a single RC parallel circuit but rather a series of parallel RC ele-

Table I. Physical properties of the AEM membrane used in this study.

Ionic functional group	$-N^+(CH_3)_3OH^-$
Conductivity (mS/cm)	21.2
Water-uptake (%)	63.9
Ion-exchange capacity (mmol/g)	1.77 ± 0.08
Density (g cm^{-3})	1.24 ± 0.01

All measurements were made at room temperatures.

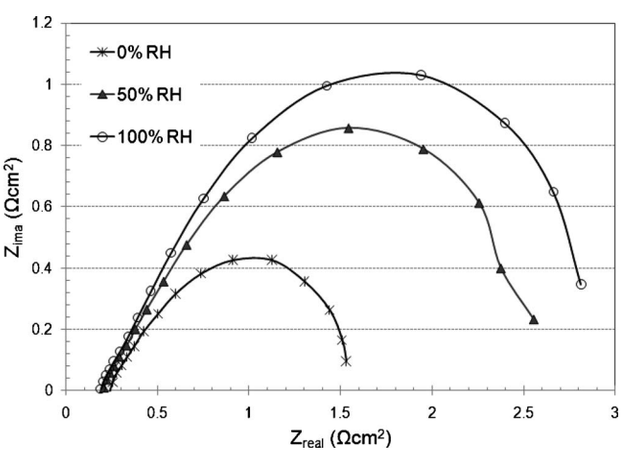

Figure 3. In situ impedance spectra of the hybrid fuel cell at 600 mV and 70°C as a function of RH.

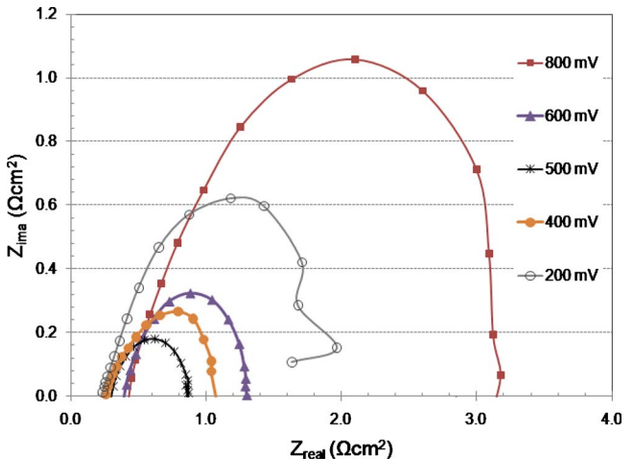

Figure 4. (Color online) In situ impedance spectra for the hybrid fuel cell at 0% RH and 70°C as a function of cell voltage.

ments due to the ever higher impedance as one moves away from the membrane into the electrode structure. The difference between the two x-intercept values of real impedance at the high and low frequency ends in Fig. 3 includes both $R_{D\Omega}$ and R_{CT} elements; however, R_{CT} is dominant. As seen in Fig. 3, R_{CT} substantially increases with higher RH of the feed gases, which is consistent with the previously reported data.[5] This change in R_{CT} with RH is attributed to flooding in the catalyst layer, as analyzed in detail below.

The high frequency x-intercept (R_{HF}) in the spectrum corresponds to the MEA's ohmic resistance. R_{HF} is largely composed of the ionic resistance of the polymer electrolyte; however, it also contains the parasitic resistance of the wires and any contact resistances. The relative comparison of R_{CT} and R_{HF} shows that the losses due to the ohmic resistance, R_{HF}, in these cells are considerably smaller than the impedance associated with the electrode assemblies. The value of R_{HF} in these hybrid cells at a fully humidified condition, 189 mΩ cm^2, is close to that of a PEM cell, 128 mΩ cm^2. This observation shows that the high conductivity of Nafion in the membrane core is largely the same here as in a PEM cell. There are two possible explanations for the higher R_{HF} value in these hybrid cells. First, the AEM ionomer in the electrode assembly has a lower ionic conductivity than the Nafion ionomer in a PEM electrode. This higher electrode resistance contributes to R_{HF} for the AEM electrode. Second, the interface between the AEM material and the PEM material is likely to form a neutral region that can increase the ionic resistance.

The sharp drop in voltage at values greater than 220 mA/cm^2 at 0% RH in Fig. 2 is unusual. Typically, the overpotential increases at high current density due to mass transfer limitations. The gas feed stoichiometries (the ratio of gas flow rate supplied at the inlet to the gas consumed at a given current density) are 2 for oxygen and 4 for hydrogen at the maximum current density. The deviation in voltage at 220 mA/cm^2 occurred at a gas feed stoichiometry higher than expected indicating that the mass transfer of reactant gas to the electrode is not the primary cause of the deviation. Figure 4 shows the impedance spectra at 0% RH for various voltage regimes. The R_{HF} value at 800 mV is larger than the ones at lower voltage probably due to the drying out of the Nafion core of the MEA because the rate of water production is lower at this potential. At lower voltages, water is produced at a high rate and hydrates the MEA resulting in a lower R_{HF}. At all voltages, the spectra exhibit a semicircular shape. The diameter of the loop initially decreases when the cell voltage is lowered to 500 mV, which is consistent with the usual behavior of the potential-dependent medium-f response (i.e., R_{CT}). In contrast, R_{CT} increases at voltages less than 500 mV, consistent with the overpotential at high current density seen in Fig. 2. Although the growth of the impedance loop is assigned to the medium-f response, the dominance of the low f response might be considered as well in the overall explanation of the change in shape in Fig. 4. It is possible to switch from the medium f dominant response at 500 mV to the low frequency response at 400 mV where diffusion of reactants and products might become dominant.[9] Further, experimental results within these transition regions in Fig. 4 are needed to clarify the exact source for the growth of the impedance loop.

The assignment of R_{CT} can be complex, particularly for the hybrid cells studied here. Typically, each electrode assembly is composed of a parallel charge-transfer resistance (R_{CT}) and double layer capacitance (RC) circuit. A parallel RC circuit element occurs at both the anode and cathode, and they together contribute to the overall charge-transfer resistance measured. One semicircular loop with a single value of R_{CT} is observed when the value of the impedance for each RC circuit is similar or the impedance is one is very small compared to the other

$$R_{CT} = R_{an} + R_{cat}$$

In a typical PEM fuel cell, R_{CT} is assigned primarily to the cathode impedance because the anode overpotential is negligible, especially at moderate current density. That is, $R_{CT} \cong R_{cat}$.[12] However, the impedance responses of the AEM anode and the AEM cathode in the hybrid cell investigated here are unknown and their individual contributions to the impedance response cannot be distinguished in the impedance data in Fig. 3 and 4. The effect of the AEM anode on the impedance spectra needs to be considered because the cell dynamics of the hybrid-cell anode is significantly altered.

To identify the individual performances of the AEM anode and AEM cathode in the hybrid cell, two different semihybrid MEAs were fabricated and compared to a conventional PEM-based MEA. The semihybrid configurations are shown in Fig. 5. The semihybrid

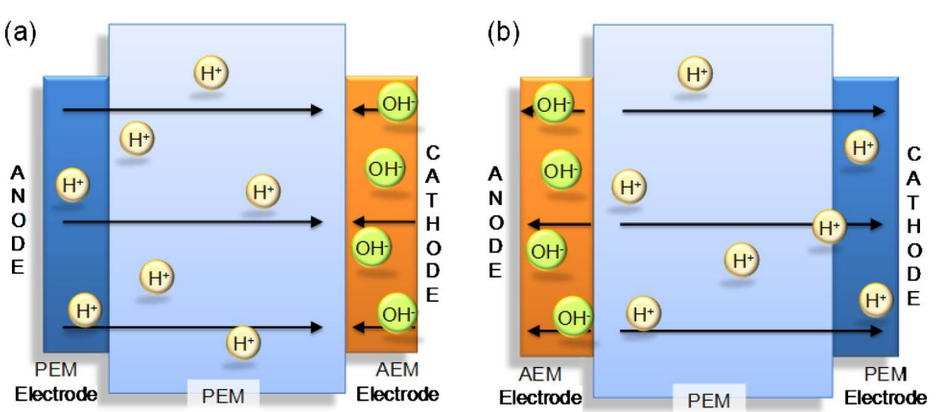

Figure 5. (Color online) A schematic of (a) CHFC and (b) AHFC semihybrid fuel cells that comprise one AEM electrode, one PEM electrode, and a proton conducting core membrane.

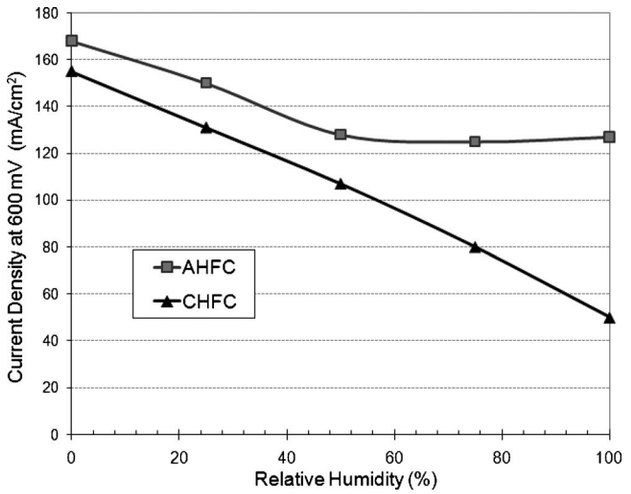

Figure 6. Current density of the semihybrid cells at 600 mV and 70°C as a function of RH. Both H_2 and O_2 gases are supplied at atmospheric pressure with flow rates of 6 and 8 sccm, respectively.

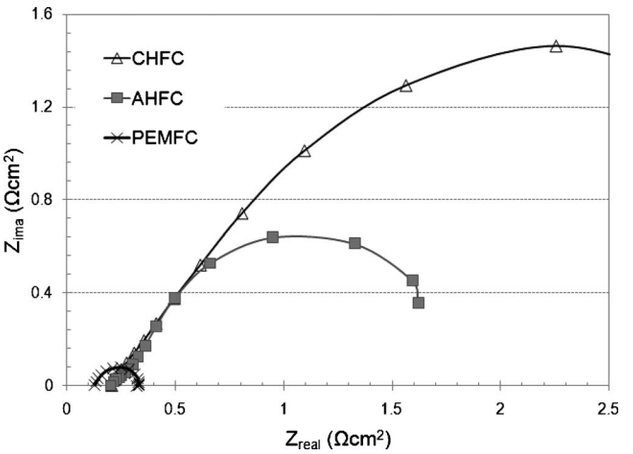

Figure 7. In situ ac impedance spectra of CHFC, AHFC, and PEMFC cells at 600 mV and 70°C at fully humidified condition.

MEAs had a PEM core between electrodes with the two different combinations of AEM and PEM electrodes. The first semihybrid configuration was comprised of an AEM-based cathode and a PEM-based anode. This cell is designated as a cathode hybrid fuel cell (CHFC). The second configuration is the reverse of the first one with an AEM-based anode and a PEM-based cathode, designated as an anode hybrid fuel cell (AHFC). These two semihybrid cells were compared to a conventional PEM-based MEA, designated as proton exchange membrane fuel cell (PEMFC). The thermodynamics of these semihybrid configurations have been evaluated recently.[7] Even though the electrode standard potentials shift due to pH difference, this potential change is offset by the junction potentials, yielding to 1.2 V cell voltage. The current densities of the two semihybrid configurations at 600 mV steady-state operation are shown in Fig. 6 as a function of RH. In both configurations, the cell performance increases as the RH decreased, similar to the behavior of the hybrid cell in Fig. 2. The AHFC has higher performance than CHFC at all RH values, with a maximum current density of 168 and 155 mA/cm^2, respectively, at dry conditions. The PEMFC had a current density of >700 mA/cm^2 at the same conditions (not included in Fig. 6). Clearly, the use of alkaline AEM electrodes as the anode or cathode rather than conventional PEM electrodes results in lower performance. This is contrary to the expected higher performance in the AEM electrodes compared to PEM electrodes because the reaction kinetics at high pH values in the AEM electrode are faster than at low pH values in the PEM electrodes.[13,14]

Further analysis of the semihybrid cells was made by comparing EIS results. Figure 7 shows the impedance response of the semihybrid and PEM cells. The R_{HF} values for the AHFC and CHFC are 202 and 207 mΩ cm^2, respectively. As seen in Fig. 7, the performance loss due to the ohmic resistance of the core PEM membrane for the semihybrid MEA is minimal compared to the increase in R_{CT}. The value of R_{CT} of the PEMFC (difference between the two x-intercepts) is substantially less than the values for the two semihybrid configurations. These data clearly show that the performance loss for the semihybrid cells is associated with the limited performance of the AEM electrodes

A comparison of the PEMFC performance to that of the CHFC and AHFC cells allows for identification of the individual contributions of the AEM anode and AEM cathode in the cell impedance because only one electrode was changed from the PEMFC in each of the semihybrid cases. The charge-transfer resistances of the AHFC and CHFC cells are composed of one AEM and one PEM electrode

$$R_{CT}^{CHFC} = R_{an,PEM} + R_{cat,AEM}$$

$$R_{CT}^{AHFC} = R_{an,AEM} + R_{cat,PEM}$$

It is recognized that the anode impedance in the PEMFC is negligible and the impedance response of the PEMFC arises primarily from the PEM cathode, $R_{CT}^{PEMFC} \cong R_{cat,PEM}$. Thus, the response of the PEM anode and cathode electrodes in the semihybrid cells can be estimated from the impedance spectra of the PEMFC with the PEMFC cathode dominating the impedance of that cell. The anode in the CHFC is composed of a PEM electrode and its impedance response is again negligible (just as it is in the PEMFC), i.e., $R_{an,PEM}^{CHFC} \cong R_{an,PEM}^{PEMFC} \cong 0$. Thus, the AEM cathode is solely responsible for the charge-transfer cell impedance of the CHFC, $R_{CT}^{CHFC} \cong R_{cat,AEM}^{CHFC}$.

Similarly, the cathodes of the AHFC and PEMFC are the identical and the cathode impedance response should be the same, $R_{CT}^{PEMFC} \cong R_{cat,PEM}^{PEMFC} \cong R_{cat,PEM}^{AHFC}$. By comparing the AHFC and PEMFC spectra, the impedance of the PEM cathode for the PEMFC (Fig. 7) is smaller than the total cell impedance of AHFC, $R_{CT}^{AHFC} \gg R_{cat,PEM}^{PEMFC} \cong R_{cat,PEM}^{AHFC}$. Thus, it is reasonable to conclude that the impedance of the AEM anode is greater than that of the PEM cathode for the AHFC, $R_{an,AEM}^{AHFC} \gg R_{cat,PEM}^{AHFC}$.

This comparison of the hybrid, semihybrid, and PEM cells shows that the AEM electrodes are the limiting components in both configurations of the semihybrid cells. In particular, it is surprising to have such a high R_{CT} for the hydrogen-fed AEM anode. Hydrogen has facile oxidation kinetics at high overvoltages, while R_{CT} is generically determined by interfacial reaction kinetics but is also a function of the three-phase contact area in the catalyst layer because the platinum catalyst has come into contact with the electrolyte, the gas feed, and the electrically conductive carbon network. R_{CT} consists of a purely kinetic term, R_{CT}^0 and is inversely proportional to the active surface area, A^0

$$R_{CT} = R_{CT}^0/A^0$$

Even though R_{CT} includes an intrinsic area term, the true surface area factor is commonly omitted in the literature in favor of the superficial area. It is more difficult to determine the true surface area in a particular operating fuel cell than the superficial area. Thus, in this paper, the unit of R_{CT} is also reported as Ω cm^2 considering the geometric, superficial surface area of the electrode and not the catalytic surface area.

The active surface area is different from the platinum surface area because not all the platinum fulfills the three-phase boundary criteria. The catalyst utilization efficiency (i.e., active surface area)

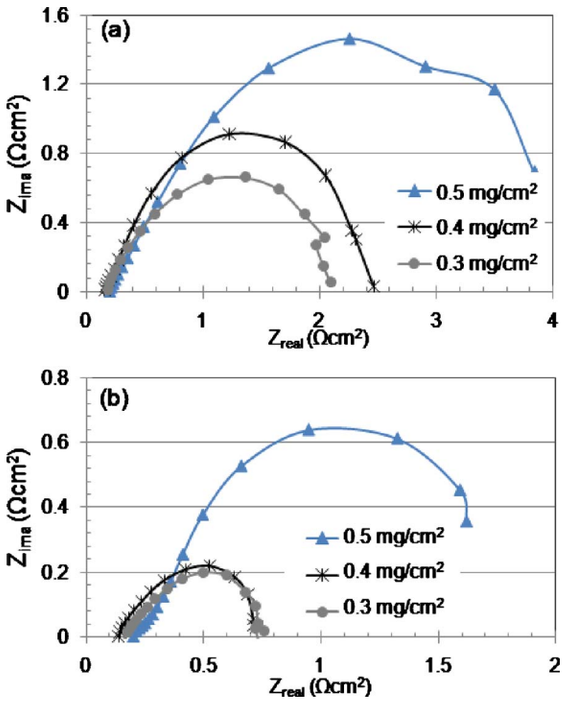

Figure 8. (Color online) In situ impedance spectra of (a) CHFC and (b) AHFC at 600 mV and 70°C for the ionomer loadings of 0.3, 0.4, and 0.5 mg/cm^2 in AEM electrodes.

largely depends on the ohmic and diffusion limitations in the catalyst layer. The properties of ionomer and its content in the catalyst layer play important roles in achieving optimum catalyst utilization.[15] Excess or insufficient ionomer content and high water content can decrease the active surface area leading to a large value of R_{CT}.

The effect of the ionomer content was initially considered for the semihybrid cells. The ionomer content in the AEM electrodes were changed while the PEM electrode composition remained constant. Figure 8 shows the impedance spectra for different ionomer loadings for the CHFC and AHFC cells. The R_{CT} value generally decreases as the ionomer content decreases for both cells. This change is more substantial for CHFC than AHFC. An important observation in the impedance spectra is that the linear response at the high-f response in Fig. 8a becomes more distorted in Fig. 8b, as the ionomer content decreases. These observations suggest that the high ionomer content lowers the contact between the catalyst particles. This leads to two major effects: (*i*) There is inaccessible catalyst surfaces, i.e., high R_{CT}, and (*ii*) the resistance in the catalyst layer is highly distributed, i.e., linear relationship at high frequency.

Even though the R_{CT} values are smaller with lower ionomer content in the AEM electrodes, they are still substantially greater than the ones in PEM electrodes, especially for the cathode (i.e., comparison of Fig. 8 to the R_{CT} value of PEMFC in Fig. 7). Additional experiments were conducted to evaluate the effect of water content on the electrode impedance in CHFC. Although high water content can facilitate high ionic conductivity, it may slow the diffusion of the gas reactants to the catalyst and block the catalyst sites reducing the active catalyst area. In a control experiment, oxygen in the cathode stream was diluted with nitrogen keeping the oxygen flow rate the same. This increased the total flow rate of the gas to the cathode. The anode flow rate was kept at 10 sccm. The higher gas flow rate to the cathode facilitates water evaporation from the electrode layer. The CHFC was initially run with the cathode flow rate of 6 sccm oxygen at 600 mV for 24 h. Then, the flow rate was increased by adding nitrogen to the cathode stream. The impedance measurements at 600 mV for nitrogen flow rates of 0, 3, and 6 sccm, after 24 h of steady-state operation are shown in Fig. 9. When the nitrogen flow rate increased, R_{CT} decreased despite the lower oxygen partial pressure at the cathode. These data show that water removal from the electrode layer increases the catalytic area that is accessible by oxygen. This is consistent with the higher performance observed at lower RH, as shown in Fig. 3. The water content in the catalyst layer decreases at low RH conditions resulting in a more active surface area, i.e., lower R_{CT}. Similarly, the larger loops observed at low voltages in Fig. 4 probably arises from the decrease in the active area by flooding due to faster water generation at high current densities.

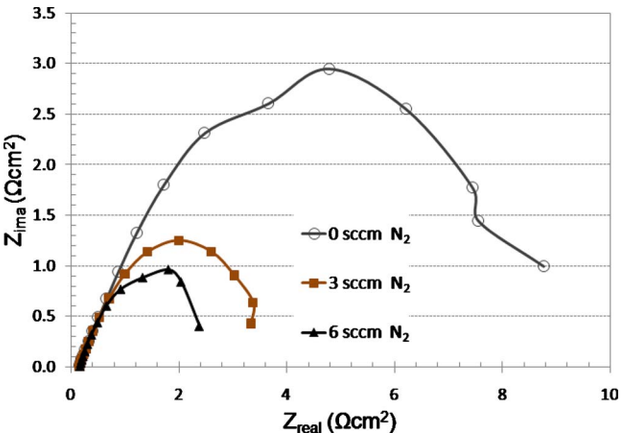

Figure 9. (Color online) In situ impedance spectra of CHFC at 600 mV and 70°C for additional N_2 flow rates of 0, 3, and 6 sccm in the cathode stream. The hydrogen and oxygen flow rates are kept constant at 10 and 6 sccm, respectively.

The data presented above is consistent with the concept that the active catalytic surface area is the rate-limiting factor in the alkaline electrodes. High catalyst utilization efficiency requires a delicate balance of several materials and processing factors including mass transport of reactants and products, ionic conductivity, and electronic conduction within the carbon network. Physical properties of the polymer electrolyte largely establish the dynamics in the catalyst layer. Specifically, the water uptake and phase segregations (i.e., forming a porous matrix) are likely to play an important role in obtaining an optimum three-phase contact area. The AEMs used here have considerably higher water uptake (63.9%) than Nafion (23%) at the equivalent conditions. Additionally, phase segregation is not likely to occur for the AEM structures used here because the pendant chain length is short.[8] Additional experimental studies are underway to evaluate the AEM materials and features needed to achieve high performance hybrid fuel cell operation.

Conclusions

The electrochemical analysis of the hybrid polymer electrolyte membrane fuel cell with alkaline electrodes and acidic core membrane was performed. The maximum power density was 131 mW/cm^2 at 70°C and 0% RH for the H_2/O_2 cell. EIS results showed that the electrode impedances limit the performance and that the ohmic resistance of the membrane was minimal. To separate the individual performances of AEM electrodes at the anode and cathode, semihybrid cells with one AEM electrode and one PEM electrode were constructed and compared to a conventional PEM-based cell. Both the AEM anode and cathode limited the performance of hybrid cells.

EIS was used to characterize the impact of the physical properties of polymer electrolyte as an electrode binder. The effect of

catalyst utilization was clearly identified on the medium-f response in the impedance spectrum. This study addresses the needs in AEM development studies.

Acknowledgment

The authors gratefully acknowledge the assistance of Vijai Narayanan in the experimental portion of this research. The financial support the Army Research Laboratory, contract LCHS22067, is also gratefully acknowledged.

Georgia Institute of Technology assisted in meeting the publication costs of this article.

References

1. J. R. Varcoe and R. C. T. Slade, *Fuel Cells*, **5**, 187 (2005).
2. J. R. Varcoe, R. C. T. Slade, G. L. Wright, and Y. Chen, *J. Phys. Chem. B*, **110**, 21041 (2006).
3. J. S. Spendelow, J. D. Goodpaster, P. J. A. Kenis, and A. Wieckowski, *J. Phys. Chem. B*, **110**, 9545 (2006).
4. C. Tamain, S. D. Poynton, R. C. T. Slade, B. Carroll, and J. R. Varcoe, *J. Phys. Chem. C*, **111**, 18423 (2007).
5. M. Ünlü, J. Zhou, and P. A. Kohl, *Fuel Cells*, **10**, 54 (2010).
6. M. Ünlü, J. Zhou, and P. A. Kohl, *Angew. Chem., Int. Ed.*, **49**, 1299 (2010).
7. M. Ünlü, J. Zhou, and P. A. Kohl, *J. Phys. Chem. C*, **113**, 11416 (2009).
8. J. Zhou, M. Unlu, J. A. Vega, and P. A. Kohl, *J. Power Sources*, **190**, 285 (2009).
9. T. E. Springer, T. A. Zawodzinski, M. S. Wilson, and S. Gottesfeld, *J. Electrochem. Soc.*, **143**, 587 (1996).
10. T. E. Springer and I. D. Raistrick, *J. Electrochem. Soc.*, **136**, 1594 (1989).
11. X.-Z. Yuan, A. Dicks, C. Song, H. Wang, and J. Zhang, *Electrochemical Impedance Spectroscopy in PEM Fuel Cells*, 1st ed., Springer, New York (2009).
12. N. Wagner, W. Schnurnberger, B. Müller, and M. Lang, *Electrochim. Acta*, **43**, 3785 (1998).
13. J. S. Spendelow and A. Wieckowski, *Phys. Chem. Chem. Phys.*, **9**, 2654 (2007).
14. K. L. Hsueh, E. R. Gonzalez, and S. Srinivasan, *Electrochim. Acta*, **28**, 691 (1983).
15. S. Litster and G. McLean, *J. Power Sources*, **130**, 61 (2004).